

# Jost function method approach for study of unstable nuclei

**Hiroshi Masui**

Information Processing Center, Kitami Institute of Technology, 165 Koen-Cho, Kitami,  
090-8507, Japan

E-mail: [hgmasui@mail.kitami-it.ac.jp](mailto:hgmasui@mail.kitami-it.ac.jp)

**Abstract.** We have developed the formalism of the Jost function method (JFM) to study unstable nuclei. We apply the JFM to the calculations, the partial decay widths in the coupled-channel problem, anti-bound (virtual) states, non-local potentials and Lagrange-mesh method. The results are compared with other methods, and we show the JFM formalism is useful to study the unstable nuclei.

## 1. Introduction

The component of the unbound states becomes important in the field of quantum systems where open channels are included in the system, e.g. study of unstable nuclei. From the aspect of the few-body treatment, the position of the  $S$ -matrix pole is a crucial key to characterize the system. The pole position can be obtained very precisely by using the Jost function method (JFM). A practical recipe for the numerical treatment of JFM was given by Sofianos and Rakityanskiy [1]. We also have developed the formalism of the Jost function method (JFM) to study the partial decay widths in coupled-channel systems [2], virtual (anti-bound) states [3], non-local kernels in the Hamiltonian [4] and application to the Lagrange-mesh formalism [5].

We have developed the applications of JFM for studying the unstable nuclei. First, we have apply the partial decay widths in a coupled-channel system can be determined by JFM under the assumption that the sum of the partial widths becomes the total width [2]. We demonstrate how accurately we can determine the partial decay widths even for broad resonant cases and show that two different schemes to define the widths give exactly the same result using the JFM approach.

Next important progress on the study of unstable nuclei is the discussion of the virtual state pole within the other physical observable, i.e. scattering phase-shift and scattering length. We compare the two systems,  ${}^5\text{He}$  and  ${}^{10}\text{Li}$  [3], which are considered to be the subsystem of halo nuclei:  ${}^6\text{He}$  and  ${}^{11}\text{Li}$ . To understand the structure of  ${}^{11}\text{Li}$ , the position of the pole in  $s$ -wave state of  ${}^{10}\text{Li}$  is important. Because  ${}^{11}\text{Li}$  is a  $p$ -shell nucleus in the shell model point of view, and the valence neutrons are in the  $0p_{1/2}$ -orbit with respect to the  ${}^9\text{Li}$  core. Nevertheless, experiments indicate the strong  $s$ -wave component for the low-lying state of  ${}^{10}\text{Li}$  ( ${}^9\text{Li}+n$ ) system, and no  $s$ -wave bound states are observed. Hence, such the  $s$ -state can be considered as a virtual (anti-bound) state. For the theoretical approach to study of  ${}^{11}\text{Li}$ , we need to determine the potential strength of the  ${}^9\text{Li}+n$  system. The position of the  $S$ -matrix pole can be investigated by JFM even for the virtual states, and we discuss how the pole moves on the complex momentum plane

by changing the potential strength. The results are connected to other physical observable such as the phase shift and scattering length.

The remaining issues for the JFM approach is to include non-local potentials or kernels into the formalism [4]. We proposed a practical approach for solving an integro-differential equation of JFM. Using this formalism, the virtual state of  $^{10}\text{Li}$  can be determined including the non-local Pauli projection operators under the orthogonality condition model.

Recently, we apply JFM to the Lagrange-mesh approach [5]. The prominent advantages of the Lagrange-mesh approach are follows. The mesh points of this method can be taken very small number compared to the conventional numerical integration for solving the differential equation, e.g. the Runge-Kutta method. The typical number of the mesh points is at most 100. Furthermore, the mesh points are defined as the zero-point of the Lagrange polynomials. Hence, the non-local potential which induces the integration in the differential equation can be reduced to a value to each mesh point.

## 2. Formalism of the Jost function method

We briefly review the Jost function method (JFM). Details are shown in Refs. [1, 2]

We consider the Schrödinger equation for the radial part of a one- or two-body system as follows:

$$\left[ \frac{\partial^2}{\partial r^2} + k^2 - \frac{2\eta k}{r} - \frac{l(l+1)}{r^2} \right] \phi(r) = \frac{2\mu}{\hbar^2} V(r) \phi(r) , \quad (1)$$

where the radial part of the wave function  $R(r)$  is replaced as  $u(r) = rR(r)$ . The homogeneous solution  $H_l^{(\pm)}(z)$  of Eq. (1) becomes known functions, i.e.  $F_l$  and  $G_l$ ; the regular and irregular Coulomb functions and  $j_l$  and  $n_l$ ; spherical Bessel functions.

In order to solve Eq. (1), we introduce two unknown functions  $\mathcal{F}^{(\pm)}(k, r)$  and define the regular solution as follows:

$$u(r) \equiv \frac{1}{2} \left[ H_l^{(+)}(kr) \mathcal{F}^{(+)}(k, r) + H_l^{(-)}(kr) \mathcal{F}^{(-)}(k, r) \right] . \quad (2)$$

The functions  $\mathcal{F}^{(\pm)}(k, r)$  become a constant for  $r \rightarrow \infty$  that correspond to the Jost functions. Since we introduced two unknown functions  $\mathcal{F}^{(\pm)}(k, r)$  for solving the equation, we can define a constraint to reduce the degrees of freedom. Thus we define the constraint as

$$H_l^{(+)} \left[ \partial_r \mathcal{F}^{(+)} \right] + H_l^{(-)} \left[ \partial_r \mathcal{F}^{(-)} \right] = 0 . \quad (3)$$

Inserting Eq. (2) into Eq (1) and using the condition (3), the second-order differential equation (1) is reduced to the first-order one:

$$\frac{\partial \mathcal{F}^{(\pm)}(k, r)}{\partial r} = \pm \frac{\mu}{ik\hbar^2} H_l^{(\mp)}(kr) V(r) \left\{ H_l^{(+)}(kr) \mathcal{F}^{(+)}(k, r) + H_l^{(-)}(kr) \mathcal{F}^{(-)}(k, r) \right\} . \quad (4)$$

This is the basic equation of the Jost function method, and we can solve the equation using ordinary numerical techniques such as the Runge-Kutta method.

For the boundary condition of the function  $\mathcal{F}^{(\pm)}(k, r)$ , we have

$$\lim_{r \rightarrow 0} \mathcal{F}^{(\pm)}(k, r) = 1 , \quad (5)$$

due to the boundary condition that the wave function is regular at the origin.

## 3. Applications of JFM to study of unstable nuclei

In this section, we show examples of the application of JFM to the study of unstable nuclei and related subjects.

### 3.1. Partial decay widths

We discuss the treatment of the partial decay widths of coupled-channel systems using a numerical example, the Noro-Taylor model [6]. The potential part of the Noro-Taylor model in the two-channel system is taken as

$$V_{nn'} = \lambda_{nn'} r^2 \exp(-r) + E_n \delta_{nn'} , \quad (6)$$

where the  $\lambda_{nn'}$  are potential strengths

$$\lambda_{nn'} = \begin{pmatrix} -1.0 & -7.5 \\ -7.5 & 7.5 \end{pmatrix} , \quad (7)$$

and  $E_n$  are the threshold energies  $E_1 = 0$  and  $E_2 = 0.1$ . The reduced masses are taken as  $\hbar^2/\mu_n = 1$ . Here all units are taken as a.u.

We calculate the resonant poles of the Noro-Taylor model using JFM and list the result in table 1. Different from the complex scaling method approach, JFM can give the complex energy of the poles even for very broad resonant states as shown in table 1.

**Table 1.** Resonant poles of the Noro-Taylor model [6] on the complex energy plane. All units are in a.u.

pole	$E_r$	$\Gamma$
1	4.768197	$1.420192 \times 10^{-3}$
2	7.241200	1.511912
3	8.171216	6.508332
4	8.440526	12.56299
5	8.072642	19.14563
6	7.123813	26.02534
7	5.641023	33.07014

Next, we discuss the calculational schemes for the partial decay widths using JFM. We compare the three different schemes for the partial decay widths, (i) the  $S$ -matrix scheme, (ii) the  $T$ -matrix scheme, and (iii) the current density scheme.

For a well-isolated resonant state, an  $S$ -matrix  $S_{nn'}(E)$  is expressed in the Breit-Wigner form with a resonance energy  $E_r$ , a total width  $\Gamma$ , and partial decay widths to channels  $n$  and  $n'$  ( $\Gamma_n$  and  $\Gamma_{n'}$ , respectively) as

$$S_{nn'}(E) \equiv S_n^{\text{bg}}(E) \delta_{nn'} - i \frac{\sqrt{\Gamma_n \cdot \Gamma_{n'}}}{E - E_r + i\Gamma/2} . \quad (8)$$

From Eq. (8), the ratio of the partial decay widths can be expressed using the ratio of the  $S$ -matrix as follows:

$$\frac{\Gamma_n}{\Gamma_{n'}} = \left| \frac{\lim_{E \rightarrow E_{\text{res}}} (E - E_{\text{res}}) S_{nn}(E)}{\lim_{E \rightarrow E_{\text{res}}} (E - E_{\text{res}}) S_{n'n'}(E)} \right| = \left| \frac{S_{nn}(E_{\text{res}})}{S_{n'n'}(E_{\text{res}})} \right| = \left| \frac{\sum_m \mathcal{F}_{nm}^{(+)}(E_{\text{res}}, \infty) \cdot \mathcal{G}_{mn}(E_{\text{res}})}{\sum_m \mathcal{F}_{n'm}^{(+)}(E_{\text{res}}, \infty) \cdot \mathcal{G}_{mn'}(E_{\text{res}})} \right| . \quad (9)$$

Here, we use the definition of the  $S$ -matrix using JFM as

$$\left( \|\mathcal{F}^{(-)}(E, \infty)\|^{-1} \right)_{mn} = \frac{1}{\det \|\mathcal{F}^{(-)}(E, \infty)\|} \mathcal{G}_{mn}(E) , \quad (10)$$

where  $\|\mathcal{G}(E)\|$  is an adjoint matrix of  $\|\mathcal{F}^{(-)}(E, \infty)\|$ . In the above expression, the origin of the pole in the  $S$ -matrix comes from the root of  $\det\|\mathcal{F}^{(-)}(E_{\text{res}}, \infty)\| = 0$ . Therefore, we can eliminate the singularity and obtain the Eq. (9). In table 2, we compare the results of three different schemes for the calculation of the partial decay widths. We show the three schemes are equivalent each other and gives the same numerical result in a good accuracy.

**Table 2.** Comparison of results for the calculation with various methods. All units are in a.u.

method	$\Gamma_1$	$\Gamma_2$
Present: $S$ -matrix	$5.1116 \times 10^{-5}$	$1.369076 \times 10^{-3}$
Present: $T$ -matrix	$5.1116 \times 10^{-5}$	$1.369076 \times 10^{-3}$
Residue of $S$ -matrix in Ref. [1]	$5.1103 \times 10^{-5}$	$1.368733 \times 10^{-3}$
Noro-Taylor [6]	$5.9 \times 10^{-5}$	$1.361 \times 10^{-3}$
$T$ -matrix in Ref. [7]	$5.1 \times 10^{-5}$	$1.368 \times 10^{-3}$
Current density in Ref. [7]	$5 \times 10^{-5}$	$1.45 \times 10^{-3}$

### 3.2. Virtual states in ${}^5\text{He}$ and ${}^{10}\text{Li}$

In this subsection, we discuss the pole position of the virtual states in  ${}^5\text{He}$  and  ${}^{10}\text{Li}$  [3].

First, we study the  $1s$ -state of the  ${}^4\text{He}+n$  system ( ${}^5\text{He}$ ), which will provide important information on the halo structure of  ${}^6\text{He}$  as a subsystem of the  ${}^4\text{He}+n+n$  model. For this purpose, we use the so-called KKNN potential [8]. Using the complex scaling method, the resonant poles of  $p$ - and  $d$ -states can be obtained. On the other hand, due to a calculational difficulty for the virtual states, the position of the poles of the  $s$ -wave states have been not investigated. Therefore, we investigate the  $s$ -wave virtual pole using JFM, which has no difficulty for calculating the virtual states. From the analysis of the phase shift and position of the poles, we conclude that the  $1s$ -state in the  ${}^4\text{He}+n$  system cannot be a virtual state without changing the scattering phase shift drastically, and even if the system becomes the virtual state, the imaginary part becomes very large.

Next, we study the  $1s$ -state in the  ${}^9\text{Li}+n$  system ( ${}^{10}\text{Li}$ ). We investigate the behavior of the  $1s$ -state pole in the  ${}^9\text{Li}+n$  system with changing the potential strength, of which we call ‘‘FP1’’. we use a parameter  $(1 + \delta)$  for the attractive part of the  ${}^9\text{Li}-n$  central potential. The trajectories of the pole of the  $1s$ -state are shown in figure 1. We take the range of the potential strength  $\delta$  from  $-0.5$  to  $0.5$ . For  $\delta = 0$ , the  $1s$ -state becomes a virtual state. The virtual state is realized in the range of the strength  $\delta$  as  $-0.26 < \delta < 0.07$ .

We compare our result for the  ${}^{10}\text{Li}$  with ones obtained by Thompson and Zhukov [9]. The result is shown in figure 2. As shown in figure 2, for the poles of P1 to P4, these positions are sensitive to the potential strength, since if we vary the strength with a very small value, the pole easily changes its position. The poles of P1 to P4 correspond our FP1 in the range of  $0 < \delta < 0.07$ .

### 3.3. Non-local operators

We consider the general case for an energy independent non-local potential  $\Lambda(r, r')$  by taking

$$V(r) \Rightarrow V(r)\delta(r, r') + \Lambda(r, r') . \quad (11)$$

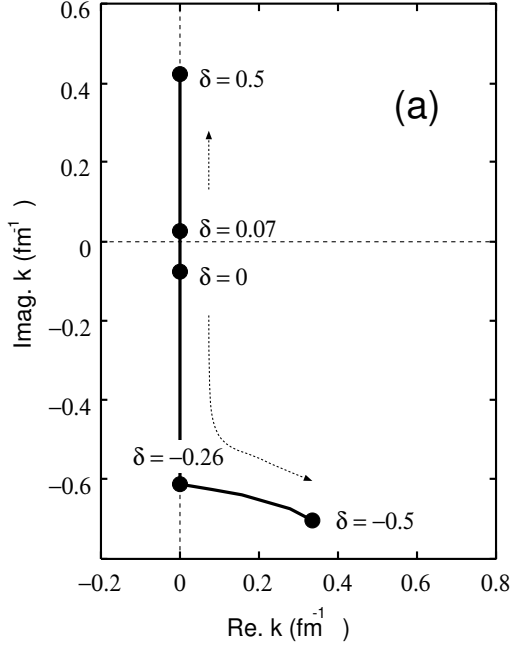


**Figure 1.** Pole behavior for  $^{10}\text{Li}$  on the complex momentum plane.

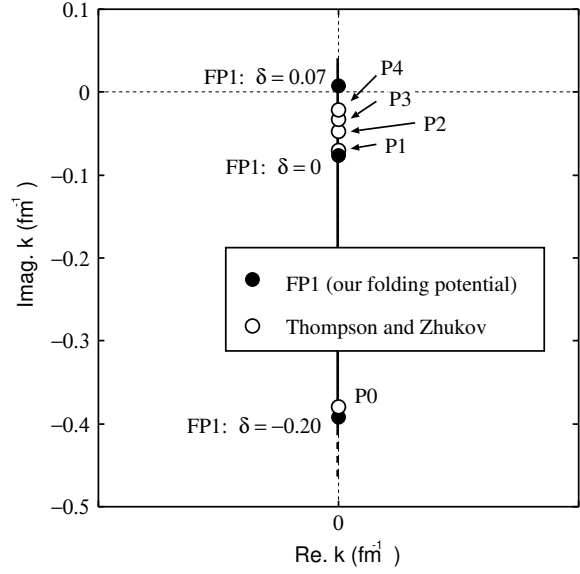


**Figure 2.** Comparison of the position of the poles with FP1 and those obtained in Ref. [20] (P0-P4).

Hence, the Schrödinger equation becomes the following form:

$$(E - \hat{H})|\phi\rangle = \hat{\Lambda}|\phi\rangle. \quad (12)$$

Using the JFM formalism, we obtain the integro-differential equation as

$$\begin{aligned} \frac{\partial \mathcal{F}_{nm}^{(\pm)}}{\partial r} &= \sum_{n'=1}^N \left[ G_{nn'}^{(\pm,+)}(r) \mathcal{F}_{n'm}^{(+)}(k_n, r) + G_{nn'}^{(\pm,-)}(r) \mathcal{F}_{n'm}^{(-)}(k_n, r) \right] \\ &+ \sum_{n'=1}^N \int_0^\infty dr' \left[ K_{nn'}^{(\pm,+)}(r, r') \mathcal{F}_{n'm}^{(+)}(k_{n'}, r') + K_{nn'}^{(\pm,-)}(r, r') \mathcal{F}_{n'm}^{(-)}(k_{n'}, r') \right]. \end{aligned} \quad (13)$$

Here, in order to simplify the expression of above equation, we define  $G$  and  $K$  as follows:

$$\begin{cases} G_{nn'}^{(\pm,+)}(r) \equiv \pm \frac{\mu_n}{ik_n \hbar^2} H_n^{(\mp)}(k_n r) V_{nn'}(r) H_{n'}^{(+)}(k_n' r), \\ G_{nn'}^{(\pm,-)}(r) \equiv \pm \frac{\mu_n}{ik_n \hbar^2} H_n^{(\mp)}(k_n r) V_{nn'}(r) H_{n'}^{(-)}(k_n' r), \end{cases} \quad (14)$$

and

$$\begin{cases} K_{nn'}^{(\pm,+)}(r, r') \equiv \pm \frac{\mu_n}{ik_n \hbar^2} H_n^{(\mp)}(k_n r) \Lambda_{nn'}(r, r') H_{n'}^{(+)}(k_n' r'), \\ K_{nn'}^{(\pm,-)}(r, r') \equiv \pm \frac{\mu_n}{ik_n \hbar^2} H_n^{(\mp)}(k_n r) \Lambda_{nn'}(r, r') H_{n'}^{(-)}(k_n' r'). \end{cases} \quad (15)$$

We introduce a matrix representation for the functions in Eq. (13) defined on the mesh points and obtain the equation as follows:

$$\mathbf{F}(\mathbf{r}) = \mathbf{F}(\mathbf{0}) + \mathbf{G}(\mathbf{r})\mathbf{F}(\mathbf{r}) + \mathbf{K}(\mathbf{r}, \mathbf{r}')\mathbf{F}(\mathbf{r}'). \quad (16)$$

Finally, the matrix of the unknown function  $\mathbf{F}(\mathbf{r})$  can be solved using the matrix inversion,

$$\mathbf{F}(\mathbf{r}) = [\mathbf{1} - \mathbf{G}(\mathbf{r}) - \mathbf{K}(\mathbf{r}, \mathbf{r}')]^{-1} \mathbf{F}(\mathbf{0}) . \quad (17)$$

In order to confirm the validity of our approach, we compare the numerical result for the coupled-channel  ${}^9\text{Li}+n$  system system. Results are shown in table 3. As shown in table 3, the JFM formalism with the matrix inversion on the mesh point can provide the accurate result as compared to the complex scaling method [10, 11, 12]. Different from the CSM approach, JFM can explicitly calculate the position of the virtual state pole on both the complex energy and momentum planes. This is a great advantage of the JFM approach in the study of unstable nuclei.

**Table 3.** Resonant and virtual states of the coupled-channel  ${}^9\text{Li}+n$  system for the potential strength used in Ref. [13],  $\delta = 0.245$ . Here “b.s.” indicates the bound state and “v.s.” the virtual state.

state	CSM [13]	JFM-OCM
$s$ -waves $2^-$	-0.028 (b.s.)	-0.028 (b.s.)
$1^-$	—	-0.018 (v.s.)
$p$ -wave $2^+$	0.71( $\Gamma = 0.40$ )	0.73( $\Gamma = 0.42$ )
$1^+$	0.42( $\Gamma = 0.19$ )	0.42( $\Gamma = 0.19$ )

### 3.4. Lagrange-mesh method

Before we formulate the JFM on the Lagrange-mesh method, we briefly show the essential formalism of the method of Lagrange mesh. Details are shown in Refs. [14, 15, 16, 17, 18].

An integration of a function  $g(x)$  in the interval  $[a, b]$  can be approximated by using the Gauss quadrature,

$$\int_a^b g(x) dx \simeq \sum_{k=1}^N \lambda_k g(x_k) . \quad (18)$$

This quadrature can be defined a product of two functions as

$$g(x) \Rightarrow f_i(x) f_j(x) . \quad (19)$$

Here, the  $f_i(x)$  are the Lagrange-basis functions, which satisfy the conditions at the mesh point  $x_j$  as follows:

$$f_i(x_j) = \lambda_i^{-1/2} \delta_{ij} . \quad (20)$$

These functions are orthonormal,

$$\int_a^b f_i(x) f_j(x) dx = \sum_{k=1}^N \lambda_k f_i(x_k) f_j(x_k) = \delta_{ij} . \quad (21)$$

Using the mesh points  $x_k$  and functions  $f_i(x_k)$ , we can formulate the matrix representation of JFM as follows:

$$\mathbf{F}_\infty - \mathbf{F}_0 \simeq \mathbf{A}_G \mathbf{F}_\infty + \tilde{\mathbf{B}}_{ex}^T \tilde{\mathbf{M}}^{-1} \tilde{\mathbf{B}} \mathbf{F}_\infty . \quad (22)$$

Solving the above equation for  $F_\infty$ , we obtain

$$F_\infty = \left( \mathbf{1} - \mathbf{A}_G - \tilde{\mathbf{B}}_{ex}^T \tilde{\mathbf{M}}^{-1} \tilde{\mathbf{B}} \right)^{-1} F_0 . \quad (23)$$

At the origin, we use the condition

$$F_0 = \begin{pmatrix} \mathcal{F}^{(+)}(0) \\ \mathcal{F}^{(-)}(0) \end{pmatrix} = \mathbf{1} . \quad (24)$$

For the detailed definition of the matrix in the above equations, please see Ref. [5]. The mesh points and weights of the Gauss quadrature are shown in figure 3. Also we show the scaling factor dependence of the JFM with Lagrange-mesh method and compare with the ordinary Runge-Kutta method in figure 4.

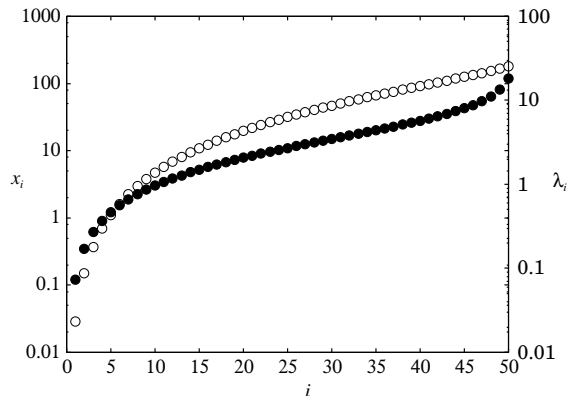


**Figure 3.** Zeros  $x_i$  (open circles) and weights  $\lambda_i$  (solid circles) of the Lagrange-Laguerre mesh.

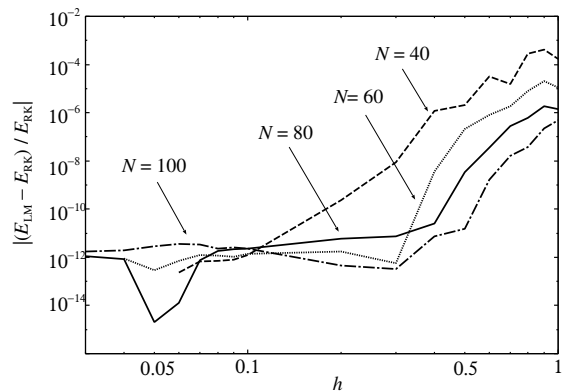


**Figure 4.** Relative errors between the Lagrange-mesh ( $E_{LM}$ ) and Runge-Kutta method ( $E_{RK}$ ) in the energies.

As a numerical example of the JFM with Lagrange-mesh method, we calculate the resonant poles of the Noro-Taylor model. The results are shown in table 4, and our approach of the Lagrange-mesh method gives a reasonable agreement to those obtained by the Runge-Kutta method. The reduction of the mesh points from Runge-Kutta to Lagrange-mesh is remarkable, e.g. an order of 10,000 to at most 100. Therefore, this method can be considered as promising for solving many coupled-channels systems.

**Table 4.** Complex eigenvalues for the Noro-Taylor model [6]. All units for the eigenvalues are in a.u.

State	JFM-LM (this work)	Ref. [2]
1	$4.768197 - i7.10096 \times 10^{-4}$	$4.768197 - i7.10096 \times 10^{-4}$
2	$7.241200 - i7.55956 \times 10^{-1}$	$7.241200 - i7.55956 \times 10^{-1}$
3	$8.171217 - i3.25417$	$8.171216 - i3.25417$
4	$8.440530 - i6.28146$	$8.440526 - i6.28150$
5	$8.072768 - i9.57315$	$8.072642 - i9.57282$

#### 4. Summary

We have developed the formalism of the Jost function method (JFM). Important quantities for the study of unstable nuclei, such as the partial decay widths, virtual states and non-local potentials can be discussed very accurately.

Our formalism for the partial decay width in the coupled-channel obtained using the ratio can avoid the singularity of the  $S$ -matrix at the complex eigen energy, and valid even for a very broad resonant states.

The position of the poles on the complex momentum plane gives an important information for the unstable nuclei. We showed the results for single- and coupled-channel cases for one of the typical unstable nuclei  $^{10}\text{Li}$ . We investigated the applicability of JFM to the non-local potential in  $^{10}\text{Li}$  case and obtained the result which agrees to the complex scaling method.

We combine the Jost function method with the Lagrange-mesh method (JFM-LM). Since the JFM-LM approach gives an accurate solution even for coupled-channel systems with 100 mesh points, it can be expected that the JFM-LM is applicable for solving the equation of the continuum discretized coupled-channel (CDCC) [19, 20]. Even though the typical number of the coupled-channel becomes more than 200 in CDCC, the total dimension of the matrix of the coupled-channel system of JFM-LM becomes  $100 \times 200 = 20,000$ . That is still feasible in practical calculations. Furthermore, for the study of many-body systems, the formalism of the JFM is applicable to the equations obtained with an expansion in hyper-spherical harmonics.

#### Acknowledgments

The author H. M would like to thank the collaborators in the study of Jost function method, K. Katō, S. Aoyama, T. Myo, and D. Baye.

#### References

- [1] Sofianos S A and Rakityansky S A 1997 *J. Phys. A* **30** 3725; 1997 *J. Phys. A* **31** 5149
- [2] Masui H, Aoyama S, Myo T and Katō K 1999 *Prog. Theor. Phys.* **102** 1119
- [3] Masui H, Aoyama S, Myo T, Katō K and Ikeda K 2000 *Nucl. Phys.* **A673**, 207
- [4] Masui H, Kurokawa C and Katō K 2003 *Prog. Theor. Phys.* **110** 233
- [5] Masui H, Aoyama S and Baye D 2013 *Prog. Theor. Exp. Phys.* **2013** 123A02
- [6] Noro T and Taylor H S 1980 *J. of Phys.* **B13** L377
- [7] Moiseyev N and Peskin U, 1990 *Phys. Rev. A* **42** 255
- [8] Kanada H, Kaneko T, Nagata S and Nomoto M, 1979 *Prog. Theor. Phys.* **61** 1327
- [9] Thompson I J and Zhukov M V 1994 *Phys. Rev. C* **49** 1904
- [10] Ho Y K 1983 *Phys. Rept.* **99** 1
- [11] Aoyama S, Myo T, Katō K and Ikeda K 2006 *Prog. Theor. Phys.* **116** 1
- [12] Myo T, Kikuchi Y, Masui H and Katō K 2014 *Prog. Part. Nucl. Phys.* **79** 1
- [13] Katō K, Yamada T and Ikeda K 1999 *Prog. Theor. Phys.* **101** 199
- [14] Baye D and Heenen P-H 1986 *J. Phys. A* **19** 2041
- [15] Vincke M, Malegat L and Baye D 1993 *J. Phys. B* **26** 811
- [16] Baye D and Vincke M 1999 *Phys. Rev. E* **59** 7195
- [17] Baye D, Hesse M and Vincke M 2002 *Phys. Rev. E* **65** 026701
- [18] Baye D 2006 *Phys. Stat. Sol. (b)* **243** 1095
- [19] Kamimura M, Yahiro M, Iseri Y, Sakuragi Y, Kameyama H and Kawai M 1986 *Prog. Theor. Phys. Suppl.* **89** 1
- [20] Austern N, Iseri Y, Kamimura M, Kawai M, Rawitscher G and Yahiro M 1987 *Phys. Rep.* **154** 125